Processing of Idiopathic Pulmonary Fibrosis images based on spatial interpolation using DFT, FFT, DCT and LPF

IRLA MANTILLA, MIHAEL ARCE
Universidad Nacional de Ingeniería,
Av. Túpac Amaru 210, Rímac, 27
PERU

Abstract: —The work focuses on the study of existing issues with some medical images obtained from patients with Idiopathic Pulmonary Fibrosis (IPF) who have survived this COVID-19 pandemic. This study analyzes potential causes of incorrect medical diagnoses with this disease. In this regard, we employ numerical algorithms such as DFT (Discrete Fourier Transform), FFT (Fast Fourier Transform), DCT (Discrete Cosine Transform), and LPF (Low-pass filter). The main objective of this work is to demonstrate that with these numerical algorithms based on Continuous and Discrete Fourier Theory, it is possible to filter existing noise in IPF radiography images. Furthermore, it is possible to compress, enhance, and improve their resolution so that better decisions can be made in a medical protocol. In this way, it contributes to the understanding of the true images that would be used for an optimal medical diagnosis.

Keywords: —Discrete Cosine Transform, Discrete Fourier Transform, Fast Fourier Transform, Idiopathic Pulmonary Fibrosis, Low-pass filter, Medical Image Processing.

Received: March 21, 2024. Revised: Agust 17, 2024. Accepted: September 20, 2024. Published: November 4, 2024.

1. Introduction

The COVID-19 pandemic has left significant consequences on the health of millions of people around the world, [1],[2]. Seven species infect humans; two from the alpha set (HCoV-229E and HCoV-NL6) and five from the beta (HCoV-HKU1, HCoV-OC43, SARS ("Severe Acute Respiratory Syndrome Coronavirus", today called SARS-CoV-1), MERS ("Middle East Respiratory Syndrome", today called MERS-CoV) and SARS-CoV 2). HCoVs infect the respiratory tract and are responsible for a certain proportion of mild respiratory tract infections that usually occur each year and are diagnosed regularly, [3]. Among the respiratory complications that have been observed in patients recovered from the disease is Idiopathic Pulmonary Fibrosis (IPF), a chronic and progressive disease that affects lung function and reduces the quality of life of those who suffer from it, [4], [5]. With the aim of better understanding the characteristics of IPF in post-COVID-19 patients, a study was carried out on the application of medical image processing techniques, [6], [7].

This study shows how medical image processing techniques can significantly contribute to improving the diagnosis of IPF and prevent patients from undergoing processes harmful to their health to obtain a diagnosis. The processing techniques used are based on the Fourier transform since it converts a spatial domain to a frequency domain; Therefore, it is possible to amplify an image, [8], by interpolating points, compressing, [8], and correcting, [9], [10], [11], an image by filtering high frequencies. We hope that the findings presented in this article will drive future research and advances in the field of IPF, thereby improving medical care and quality of life for affected patients, [12].

2. Frequency Domain Processing

The frequency domain is the realm in which an image is represented as the sum of periodic signals of different frequencies. For instance, the Fourier transform of an image is the representation of that image through a summation of complex exponentials with varying magnitudes, frequencies, and phases. The discrete one-dimensional Fourier transform and its inverse are defined as follows, [8], and, [9], respectively:

$$\mathcal{F}\{x(n)\} = F(k) = \sum_{n=0}^{N-1} x(n) e^{\frac{2\pi i}{N} kn};\ k \in \{0,1,\dots,N-1\}$$

$$\mathcal{F}^{-1}\{F(k)\} = x(n) = \frac{1}{N}\sum_{k=0}^{N-1} F(k) e^{\frac{2\pi i}{N} kn};\ k \in \{0,1,\dots,N-1\}$$

Meanwhile, the discrete l-dimensional transforms are defined as follows:

$$\mathcal{F}\{x(n_1,\dots,n_l)\} = F(k_1,\dots,k_l) = \sum_{n_1=0}^{N_1-1} \dots \sum_{n_l=0}^{N_l-1} x(n_1,\dots,n_l)\, e^{\frac{2\pi i}{N_j} k_j n_j};$$
$$k_j \in \{0,1,\dots,N_j-1\}, \quad \forall j \in \{1,2,\dots,l\}$$

$$\mathcal{F}^{-1}\{F(k_1,\dots,k_l)\} = x(n_1,\dots,n_l) = \frac{1}{\prod_{j=1}^{l} N_j}\sum_{k_1=0}^{N_1-1}\dots\sum_{k_l=0}^{N_l-1} F(k,\dots,k_l)\, e^{\frac{2\pi i}{N_j}k_j n_j};$$
$$k_j \in \{0,1,\dots,N_j-1\}, \qquad \forall j \in \{1,2,\dots,l\}$$

3. Fast convolution

An important property of the Fourier transform is that the multiplication of the Fourier transforms of two associated spatial functions is equal to the product of their individual transforms. This property, together with the fast Fourier transform, form the basis for the convolution algorithm. The discrete Fourier convolution, [8], is expressed as follows:

$$(F * G)(k) = \frac{1}{N}\sum_{n=0}^{N-1} x_1(n)x_2(n)e^{\frac{-2\pi i}{N}kn}; \;\; k \in \{0,1,\dots,N-1\}$$

Given two matrices $A_{m\times n}$ and $B_{p\times q}$ representing the values of one of the RGB components of two images, the convolution algorithm between these matrices is executed through the following steps:

1. Zeros are added to A and B to make the dimensions of the resulting matrix C from the convolution between A and B $(p+m-1)\times(q+n-1)$. Additionally, zeros are often added to A and B until the number of elements in each matrix is a power of two.
2. The two-dimensional Fourier transforms of A and B are computed.
3. The element-wise multiplication is performed between the Fourier transform of A and the Fourier transform of B.
4. The two-dimensional inverse Fourier transform is applied to the product obtained in the previous step.

4. Image Amplification

Image amplification based on spatial interpolation through the frequency domain can be carried out using the following method:

A transformation matrix $A_{J\times J}$ is defined as follows:

$$A_J = \left[a_{mn}^J\right]; \;\; a_{mn}^J = \frac{1}{J}e^{\frac{-2\pi i}{J}mn}; \;\; m,n = 0,1,2,\dots,J-1$$

The matrices $P = A_M$ and $Q = A_N$ are defined. Therefore, the discrete Fourier transform of x would be given by:

$$F = PxQ$$

Expressing the above equality using summations, the two-dimensional discrete Fourier transform is given by:

$$F(u,v) = \frac{1}{MN}\sum_{m=0}^{M-1}\sum_{n=0}^{N-1} x(m,n)e^{2\pi i(\frac{mu}{M},\frac{nv}{N})};$$
$$u = 0,1,\dots,M-1; \;\; v = 0,1,\dots,N-1$$

By defining a transformation matrix $B_{J\times J}$ as:

$$B_J = \left[b_{mn}^J\right]; \;\; b_{mn}^J = e^{\frac{2\pi i}{J}mn}; \;\; m,n = 0,1,2,\dots,J-1$$

Given that:

$$\sum_{m=0}^{J-1} e^{\frac{-2\pi i}{J}km}e^{\frac{-2\pi i}{J}mn} = \begin{cases} J; & k = n \\ 0; & k \neq n \end{cases}$$

It can be deduced that:

$$B_J^{-1} = A_J$$

Therefore, the Inverse Discrete Fourier Transform is given by:

$$x(m,n) = \sum_{u=0}^{M-1}\sum_{v=0}^{N-1} F(u,v)\, e^{2\pi i(\frac{mu}{M}+\frac{nv}{N})}$$
$$m = 0,1,\dots,M-1; \;\; n = 0,1,\dots,N-1$$

This method is quite suitable because even though the four groups of nodes are very separated, when transforming the spatial domain into a frequency domain, they remain practically equidistant so that the interpolation can be effective. Finally, we proceed to carry out the procedure for the amplification of images, [8], whose dimensions are powers of "two" due to the change of domain, as follows:

1. Place the values of the first RGB component of each pixel in the image into a matrix $Y_{M\times N} = [y_{ij}]$ according to their position in the image.
2. Apply the two-dimensional discrete Fourier transform to the matrix $Y_{M\times N}$ and store the result in a matrix $A_{M\times N} = [a_{ij}]$, assuming that $x(i-1,j-1) = y_{ij}$, and $F(i-1,j-1) = a_{ij}; \;\; \forall i = 1,\dots,M; j = 1,\dots,N$.
3. Let α be the value of the proportional increase in image dimensions. Define the matrix A_α with dimensions $\alpha M \times \alpha N$ as follows:

$$A_\alpha = [a_{ij}^\alpha] = \begin{cases} a_{ij}^\alpha = a_{ij}; \;\; i \in \left\{1,\dots,\frac{M}{2}\right\} \cup \left\{\left(\alpha-\frac{1}{2}\right)M+1,\dots,M; \right. \\ \qquad\qquad j \in \left\{1,\dots,\frac{N}{2}\right\} \cup \left\{\left(\alpha-\frac{1}{2}\right)N+1,\dots,N\right\} \\ 0; \;\; i \in \left\{\frac{M}{2}+1,\dots,\left(\alpha-\frac{1}{2}\right)M\right\}; \forall j \in \left\{\frac{N}{2}+1,\dots,\left(\alpha-\frac{1}{2}\right)N\right\} \end{cases}$$

4. Apply the inverse discrete Fourier transform to the matrix A_α to obtain the matrix Y_α with dimensions $\alpha M \times \alpha N$.

5. Multiply each element of the matrix Y_α by $1/\alpha^2$ to compensate for the increase in its values caused by the inverse transform applied to the α^2 times larger matrix A_α compared to the original matrix A.

6. Repeat the previous steps for the other two components of each pixel in the image.

In Figure 1, you can see how the matrix A_α is constructed from the matrix A in step 3:

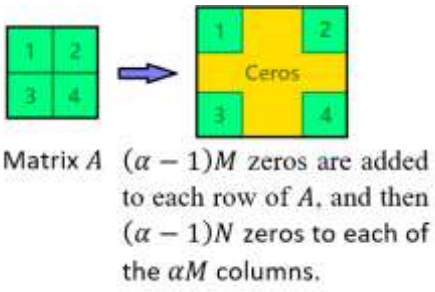

Fig. 1 Construction of the augmented matrix A_α from the matrix A

5. Discrete Cosine Transform (DCT)

The Discrete Cosine Transform (DCT) represents the values of a matrix that represents an image by summing sine waves of different amplitudes and frequencies. It is commonly used in image compression because most of the visually significant information is concentrated in only a few DCT coefficients, [8]. Given a matrix $A = [a_{ij}]$ with dimensions $M \times N$, the coefficients $b_{pq};\ p = 0,1,\dots,M;\ q = 0,1,\dots,N$ of the Discrete Cosine Transform of A are obtained as follows:

$$b_{pq} = \alpha_p \alpha_q \sum_{m=0}^{M-1} \sum_{n=0}^{N-1} \alpha_{mn} \cos\left(\frac{(2m+1)\pi p}{2M}\right) \cos\left(\frac{(2n+1)\pi q}{2N}\right)$$

Where the coefficients α_p and α_q are defined as follows:

$$\alpha_p = \begin{cases} \sqrt{\frac{1}{M}};\ p = 0 \\ \sqrt{\frac{2}{M}};\ 1 \le p \le M-1 \end{cases} \qquad \alpha_q = \begin{cases} \sqrt{\frac{1}{N}};\ q = 0 \\ \sqrt{\frac{2}{N}};\ 1 \le q \le N-1 \end{cases}$$

And the coefficients $a_{mn};\ m = 0,1,\dots,M;\ n = 0,1,\dots,N$ of the inverse Discrete Cosine Transform of the matrix $B = [b_{ij}]$ with dimensions $M \times N$ are obtained as follows:

$$a_{mn} = \sum_{p=0}^{M-1} \sum_{q=0}^{N-1} \alpha_p \alpha_q b_{pq} \cos\left(\frac{(2p+1)\pi m}{2M}\right) \cos\left(\frac{(2q+1)\pi n}{2N}\right)$$

6. Low-Pass Filter

It is a smoothing filter that attenuates or eliminates the gain of the high-frequency components and only keeps the low-frequency components unaltered (allows the low frequencies to pass), [9]. It is very effective in eliminating noise in images since these have high frequencies. high in noisy areas due to the sudden change in the RGB values of the noisy pixels and their neighboring pixels. This filter defines a function $H: \mathbb{R}^2 \to \mathbb{R}$ based on a cutoff frequency D_0 that filters points in the frequency plane by evaluating their distances from the origin. To do this, the function $D: \mathbb{R}^2 \to \mathbb{R}$ is defined as follows:

$$D(u,v) = \sqrt{u^2 + v^2}$$

The filter is executed following these steps:

1. Input: Read the image to be filtered.
2. Save the size of the input image in pixels in the processor's memory.
3. Perform the Fourier transform of the image.
4. Assign a value to the cutoff frequency D_0.
5. Define the low-pass filter function H and establish the mesh on the frequency plane of the image where it will be defined.
6. Convolve the Fourier transform of the input image with the filtering mask H.
7. Take the inverse Fourier transform of the convolved image.
8. Output: Display the resulting image.

6.1 Ideal Low-Pass Filter

It is the simplest one. This filter allows signals with frequencies lower than or equal to the cutoff frequency to pass through and rejects those with frequencies higher than the cutoff frequency, [10]. The function H is defined as follows:

$$H(u,v) = \begin{cases} 1;\ D(u,v) \le D_0 \\ 0;\ D(u,v) < D_0 \end{cases}$$

In Figure 2, you can observe the graph of the function H with respect to the mesh on the image and with respect to the distance between the point in the image where the function H is evaluated and the origin of coordinates in the frequency plane of the image. Therefore, when performing the convolution mentioned in step 6 of this filter's algorithm, it will only affect the points in the image that are located at the base of the cylinder in the first graph of this figure.

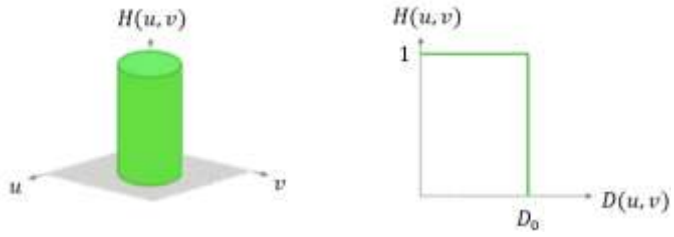

Fig. 2 Perspective plot of an ideal low-pass filter transfer function and the radial cross-section of the filter

6.2 Butterworth Low-Pass Filter of Order n

It is a type of smooth maximum attenuation filter, which means it has a gradual attenuation rather than a sharp attenuation at frequencies above the cutoff frequency. Therefore, it produces a nearly constant response until it approaches the cutoff frequency closely enough and then begins to decrease at a rate of $6n\ dB$ per octave. This makes the filter suitable for applications where a smooth transition between pass and attenuated frequencies is desired. This filter is widely used in various applications, including signal processing, system control, and noise removal, [11]. The function H is given by:

$$H(u,v) = \frac{1}{1 + \left(\frac{D(u,v)}{D_0}\right)^{2n}}$$

In Figure 3, you can see the graph of the function H with respect to the mesh on the image, and in Figure 4, you can observe the graph of the function H with respect to the distance between the point in the image where the function H is evaluated and the origin of coordinates in the frequency plane of the image for orders 1 to 5:

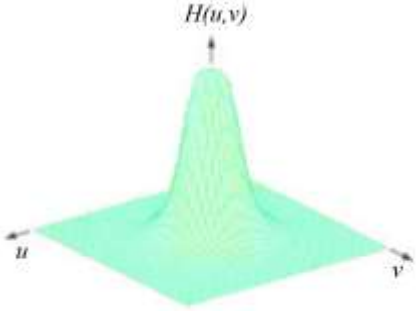

Fig. 3 Perspective plot of a Butterworth low-pass filter transfer function of order n

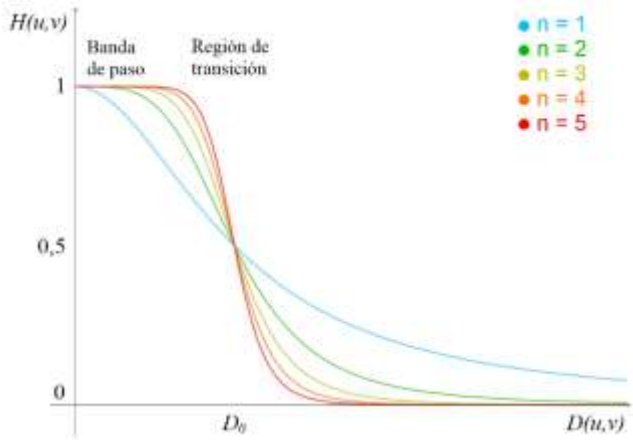

Fig. 4 Graph of the radial cross-section of the Butterworth low-pass filter of order n

6.3 Gaussian Low-Pass Filter

This filter is commonly used for image smoothing. The filter works by averaging the pixel intensity values in an image within a certain neighborhood radius around each pixel. This results in a less detailed and less noisy image, although it can also make the image appear less sharp. It is also used as a preprocessing step for other image-processing operations such as edge detection and image segmentation. This filter has a frequency response that is a Gaussian function and allows low frequencies to pass while attenuating higher frequencies, [10]. In this filter, the function H is given by:

$$H(u,v) = e^{-D^2(u,v)/(2D_0^2)}$$

In Figure 5, you can observe the graph of the function H with respect to the mesh on the image and with respect to the distance between the point in the image where the function H is evaluated and the origin of coordinates in the frequency plane of the image.

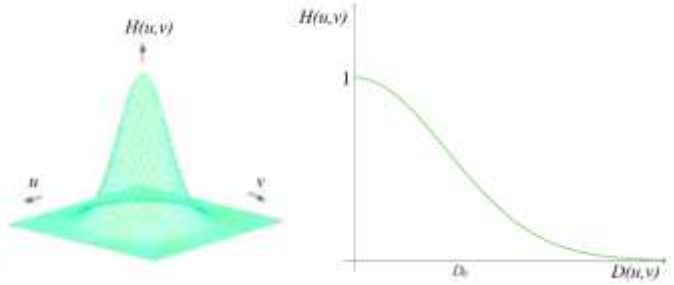

Fig. 5 Perspective plot of a Gaussian low-pass filter transfer function and the radial cross-section of the filter

7. IMPLEMENTATION

When we double the dimensions of a radiograph of IPF using a Matlab code that follows a method for enlarging images based on spatial interpolation through the frequency domain, we find that the resolution of the radiograph is maintained even after enlargement, as can be seen by comparing Figure 6, [13], with Figure 7. This process has already been successfully tested on other images before and is carried out with the aim of improving the visualization of certain areas of the image:

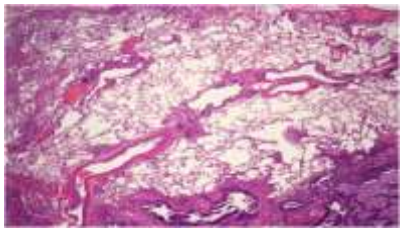

Fig. 6 Original image of an Idiopathic Pulmonary Fibrosis X-ray, [13].

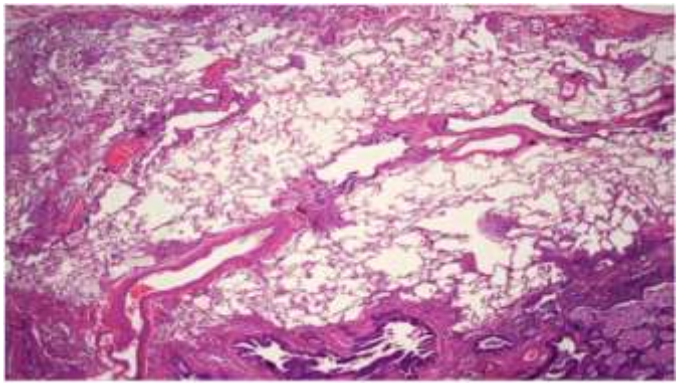

Fig. 7 Here is the result of enlarging the image from the previous figure to four times its area using spatial interpolation methods based on the Fast Fourier Transform (FFT) and Discrete Fourier Transform (DFT) for an Idiopathic Pulmonary Fibrosis X-ray.

When compressing the image from Figure 6 using the Discrete Cosine Transform (DCT) method, the result shown in

Figure 8 is obtained. This method is performed to reduce the image's file size.

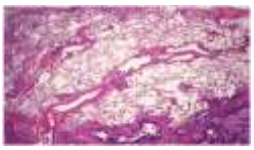

Fig. 8 Result of applying image compression based on DCT while retaining 777 coefficients and achieving a compression ratio of 5/4 to an Idiopathic Pulmonary Fibrosis X-ray.

When comparing Figure 9, [14], with Figure 10, Figure 11, and Figure 12, you can see the result of applying the ideal, Butterworth of order 3, and Gaussian Low-Pass filters, respectively, with a cutoff frequency of 90 Hz to an Idiopathic Pulmonary Fibrosis X-ray with the "salt and pepper" noise.

Fig. 9 Idiopathic Pulmonary Fibrosis X-ray with "salt and pepper" noise, [14].

Fig. 10 Effect of the ideal low-pass filter with a cutoff frequency of 90 Hz on an Idiopathic Pulmonary Fibrosis X-ray with "salt and pepper

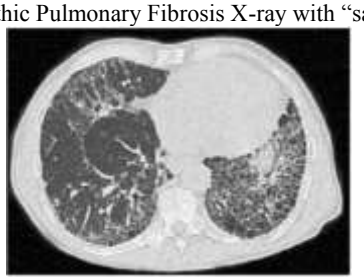

Fig. 11 Effect of the Butterworth low-pass filter of order 3 with a cutoff frequency of 90 Hz on an Idiopathic Pulmonary Fibrosis X-ray with "salt and pepper"

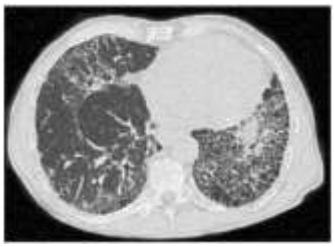

Fig. 12 Effect of the gaussian low-pass filter with a cutoff frequency of 90 Hz on an Idiopathic Pulmonary Fibrosis X-ray with "salt and pepper"

8. Conclusion

Algorithms based on the Fast Fourier Transform were successfully developed to correct errors in digital images. As a result, an Idiopathic Pulmonary Fibrosis X-ray was amplified using the method of two-dimensional Discrete Fourier Transform, as shown in Figure 6. Compression of an Idiopathic Pulmonary Fibrosis X-ray was achieved through the Discrete Cosine Transform (DCT), as demonstrated in Figure 7. Additionally, noise was effectively reduced in an Idiopathic Pulmonary Fibrosis X-ray using low-pass filters, as shown in Figures 8, Figure 9, and Figure 10. Therefore, digital images were created by applying algorithms in Matlab to Idiopathic Pulmonary Fibrosis X-rays, contributing to improved diagnosis.

References

[1] Carfì A, Bernabei R, Landi F, Gemelli Against COVID-19 Post-Acute Care Study Group. Persistent symptoms in patients after acute COVID-19. JAMA. 2020;324(6):603-605.W.-K. Chen, Linear Networks and Systems (Book style). Belmont, CA: Wadsworth, 1993, pp. 123–135.

[2] Nalbandian A, Sehgal K, Gupta A, Madhavan MV, McGroder C, Stevens JS, et al. Post-acute COVID-19 syndrome. Nat Med. 2021;27(4):601-615.

[3] Manta, B., Sarkisian, A. G., Garcia-Fontana, B., & Pereira-Prado, V. (2022). Pathophysiology of COVID-19. *Odontoestomatología, 24*(39), e312. Retrieved from: https://doi.org/10.22592/ode2022n39e312

[4] Raghu G, Remy-Jardin M, Myers JL, et al. Diagnosis of idiopathic pulmonary fibrosis: an Official ATS/ERS/JRS/ALAT Clinical Practice Guideline. Am J Respir Crit Care Med. 2018;198(5):e44-e68.

[5] Kreuter M, Swigris J, Pittrow D, et al. The clinical course of idiopathic pulmonary fibrosis and its association to quality of life over time: longitudinal data from the INSIGHTS-IPF registry. Respir Res. 2019;20(1):59.

[6] Lowe DG. Distinctive image features from scale-invariant key points. Int J Comput Vision. 2004;60(2):91-110.

[7] González RC, Woods RE. Digital Image Processing. Pearson Education; 2008.

[8] Esqueda JJ, Palafox LE. Fundamentals of image processing. Universidad Autónoma de Baja California; 2005. Available at: https://www.academia.edu/9729833/Fundamentos_de_Procesamiento_de_Imágenes_Evento_CONATEC_2002 (pp. 15-24).

[9] Smith SW. Applications of the DFT. En: Smith SW, editor. Digital Signal Processing. Newnes; 2003. p. 169-184. DOI: 10.1016/B978-0-7506-7444-7/50046-7

[10] Ramírez L, Rodríguez M. Comparative analysis of low-pass filters: Ideal, Butterworth, and Gaussian. Revista de Procesamiento de Señales. 2018;12(2):45-58. DOI: 10.1016/j.rps.2017.12.004

[11] Zhang H, Chen W. Evaluating the performance of low-pass filters: Ideal, Butterworth, and Gaussian. IEEE Trans Signal Process. 2020;68:287-301. DOI: 10.1109/TSP.2019.2948276

[12] Ley B, Collard HR, King TE Jr. Clinical course and prediction of survival in idiopathic pulmonary fibrosis. Am J Respir Crit Care Med. 2011;183(4):431-440.

[13] Giménez Palleiro A, Franquet T. Figure 13: CTMD reconstructed image in the coronal plane in a patient with sarcoidosis, showing micronodular involvement predominantly in the middle and upper fields, associated with septal thickening. In: Radiological Patterns in Interstitial Lung Disease. Elsevier; 2013. DOI: 10.1016/j.semreu.2013.05.002

[14] Neumología Peruana. (n.d.). Idiopathic pulmonary fibrosis: Now it is possible to diagnose through tomography. In Diagnosis of Idiopathic Pulmonary Fibrosis by Tomography (HRCT). Retrieved from: Diagnosis of pulmonary fibrosis - First steps (neumologiaperuana.com)

Contribution of Individual Authors to the Creation of a Scientific Article (Ghostwriting Policy)

The authors equally contributed in the present research, at all stages from the formulation of the problem to the final findings and solution.

Sources of Funding for Research Presented in a Scientific Article or Scientific Article Itself

No funding was received for conducting this study.

Conflict of Interest

The authors have no conflicts of interest to declare that are relevant to the content of this article.